Journal of Organometallic Chemistry 891 (2019) 64–71

Contents lists available at ScienceDirect

Journal of Organometallic Chemistry

journal homepage: www.elsevier.com/locate/jorganchem

Design of organoruthenium complexes for nanoparticle functionalization

Saawan Kumar, Guillaume Gallician, Dennis Weidener, Matthew P. Sullivan, Tilo Söhnel, Muhammad Hanif**, Christian G. Hartinger*

School of Chemical Sciences, University of Auckland, Private Bag 92019, Auckland, 1142, New Zealand

ARTICLE INFO

Article history:
Received 9 January 2019
Received in revised form
18 March 2019
Accepted 27 March 2019
Available online 9 April 2019

Dedicated to Prof. Armando José Latourrette de Oliveira Pombeiro on the occasion of his 70th birthday

Keywords:
Bioorganometallic chemistry
Nanoparticle functionalization
Organoruthenium complexes
Picolinamide

ABSTRACT

In recent years, extensive research efforts have been focused on loading metal complexes onto macromolecular systems such as nanoparticles. We report a ligand with a catechol group based on a picolinamide which allows for coordination to organoruthenium moieties while the catechol group remains available for loading on nanoparticles as delivery vehicles towards tumors. All the compounds were characterized with standard analytical methods and the molecular structure of the ligand **1**, and its Ru complexes **1a** and **1b** were determined by X-ray diffraction analysis. The crystal structure of **1a** and **1b** showed pseudo-tetrahedral geometry of the Ru center with "piano-stool" conformation and **1** coordinated as an *N,O*-bidentate ligand, however, the latter depending on the reaction conditions employed. The Ru complexes **1a**–**1c** were effectively loaded on magnetite nanoparticles as characterized by inductively-coupled plasma mass spectrometry (ICP-MS), transmission electron microscopy (TEM) and Fourier transform infrared spectroscopy (FTIR).

1. Introduction

In recent years, half-sandwich organoruthenium complexes have been widely investigated for their catalytic and pharmacological properties [1,2]. Their reactivity and biological activity [3,4] as well as their catalytic potential can be tailored by careful choice of the ligands [5–7]. Loading them on macromolecular systems such as dendrimers, metallacages, liposomes, and nanoparticles (NPs) equipped Ru(arene) and other metal complexes with targeting capability to the tumor [8]. When loading catalysts on macromolecular support, issues like the separation of the catalyst from the product, or recycling of the catalyst can be addressed [9], as was shown by Süss-Fink et al. for Ru/superparamagnetic iron oxide nanoparticles (SPIONs) [10] and Fan and colleagues for Ru(arene) organometallics [11]. Moreover, such modification seems to open opportunities in research areas such as single molecule magnet and molecular nanomagnet development [12,13].

SPIONs possess interesting magnetic properties, are biocompatible and biodegradable [14]. Studies have shown that SPIONs accumulate in tumors and such systems have been approved by the FDA for MRI and hyperthermia therapy [15–18], the latter also in combination with anticancer chemo- and radiotherapy [19,20]. Several examples of SPIONs as drug carriers for metal-based anticancer agents, such as cisplatin derivatives [21] and redox-responsive Pt^{IV} [22] compounds have been reported and demonstrated interesting chemical and biological properties. Macromolecules such as NPs can extravasate into tumor tissue *via* leaky blood vessels exploiting the enhanced permeability and retention (EPR) effect [23]. For example, gold NPs have been used for the delivery of the anticancer drugs cisplatin [24,25], oxaliplatin [25,26], and carboplatin [25,27].

Ru(arene) compounds with many different ligands are known and they often have interesting biological activity depending on the ligand [1,28–38]. Picolinic acid and its derivatives are frequently used as ligands to metal centers including ruthenium [39–44]. They coordinate *via* the pyridine nitrogen and either the amide nitrogen to give *N,N*-coordination or the amide oxygen to form *N,O*-

* Corresponding author. School of Chemical Sciences, University of Auckland, Private Bag 92019, Auckland, 1142, New Zealand.;
** Corresponding author.
E-mail addresses: m.hanif@auckland.ac.nz (M. Hanif), c.hartinger@auckland.ac.nz (C.G. Hartinger).
URL: http://hartinger.auckland.ac.nz

https://doi.org/10.1016/j.jorganchem.2019.03.020
0022-328X/

complexes. The coordination mode depends on the reaction conditions, such as pH and temperature, and has a strong influence on the reactivity and cytotoxicity of organoruthenium compounds [42,44], although picolinic acid derivatives show minor cytotoxic activity [45].

In this paper, we describe a strategy to specifically tag SPIONs with organometallic complexes. For that purpose, we have functionalized a picolinamide ligand with a catechol group and prepared its organoruthenium compounds with different halido ligands as leaving groups. Catechols are known to form very stable complexes with a variety of metal ions, including Fe^{III} [46,47]. Therefore, this anchoring system is particularly well-suited to load an organometallic moiety on NPs. The prepared organoruthenium compounds were characterized with different analytical methods including X-ray diffraction analysis. The complexes were loaded on magnetite (Fe_3O_4) NPs and the organoruthenium-NP conjugates were characterized by ICP-MS, FTIR, and TEM.

2. Results and discussion

In order to be able to functionalize Fe_3O_4 NPs with an organometallic Ru(arene) moiety, the picolinamide derivative **1** was designed which allows for coordination to metal centers through its pyridine *N* donor and the amide oxygen or nitrogen atoms in a bidentate manner, as has been observed for other picolinamide derivatives [43]. However, organoruthenium-picolinic acid complexes have been shown to be relatively non-cytotoxic [45]. In addition, **1** contains a catechol group known for its ability to chelate iron, in particular in oxidation state +3 [47]. This will allow organoruthenium complexes bind to the surface of Fe_3O_4 NPs. The synthesis of *N*-(3,4-dihydroxyphenethyl)picolinamide **1** was accomplished by the coupling of 3,4-dihydroxyphenethylamine and 2-pyridine carboxylic acid using HATU as an amide coupling reagent (Scheme 1). Compound **1** was obtained as a white solid after extraction and column chromatography in a yield of 37%. The reactions were conducted in the dark and under inert conditions using degassed solvents and thoroughly dried reagents as the catechol group can be oxidized to the respective orthoquinone [48]. The ^{1}H and ^{13}C{^{1}H} NMR spectra showed characteristic signals assignable to the pyridine and dopamine fragments. The most downfield peak in the ^{1}H NMR spectrum at δ 8.58 ppm was assigned to the proton adjacent to the pyridine nitrogen (H1). ESI-MS gave peaks with *m*/*z* values corresponding to the $[M + H]^+$ and $[M + Na]^+$ ions, the latter representing the base peak in the spectrum.

Compound **1** being only slightly soluble in water was crystallized from water in a triclinic crystal system, with an inversion

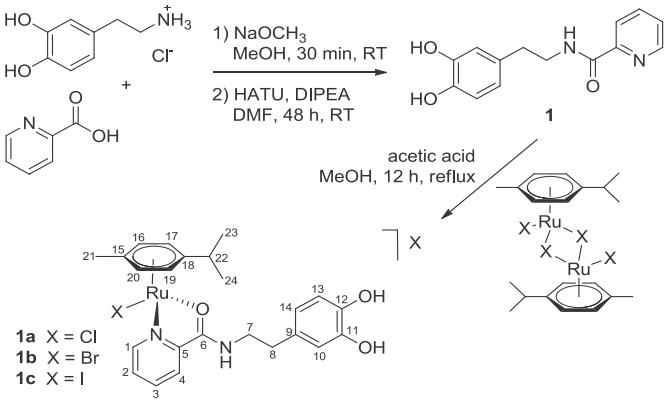

Scheme 1. Synthetic route to **1** and its Ru complexes **1a**–**1c**.

center and space group *P*-1. The flexible nature of the aliphatic linker between the picolinamide and the catechol group results in two crystallographically independent molecules in the unit cell. While the first structure features parallel aromatic rings, in the second molecule a bent arrangement was observed (Fig. S1). The molecules with parallel aromatic groups form two hydrogen bonds with each other involving the picolinamide oxygen atom $O1_p$ and one of the two catechol hydroxyl groups ($O2_p$–H···$O1_p$). The second catechol hydroxyl group ($O3_p$–H) is involved in a hydrogen bonding network and bonds to the $O3_b$–H of a neighboring bent molecule **1**, which in turn forms a hydrogen bond to the $N1_p$ of another molecule with parallel aromatic rings, which is also involved in a hydrogen bond between $N2_b$–H and $O3_b$–H of the same bent structure (Fig. 1). Two bent molecules form another set of hydrogen bonds with each other ($O2_b$–H···$O1_b$). Two molecules of **1** with parallel arrangement of the phenyl and pyridine rings form π interactions and the shortest distance between the pyridine rings involved in the π interactions was 3.396 Å (Fig. S2).

To prepare the desired [Ru(cym)(**1**)X]X (cym = η^6-*p*-cymene) complexes with the respective halido ligands **1a**–**1c** (X = Cl, Br or I), **1** was refluxed with stoichiometric amounts of the dimeric ruthenium precursors $[Ru(cym)X_2]_2$ (Scheme 1) in dry methanol for 12 h. ^{1}H NMR spectroscopy indicated the presence of a mixture of two species. This can be explained by ligand **1** possessing two possible bidentate coordination modes, *i.e.*, through the pyridine nitrogen and either the amide nitrogen (*N,N*) or oxygen (*N,O*) atoms. In this case, the product in which **1** was *N,O*-coordinated to the Ru center was identified as the major product. To favor formation of the *N,O*-coordinated complex, acetic acid was used to acidify the solution to a pH value of 3. The addition of acetic acid ensured that only *N,O*-coordination was observed as the amide nitrogen remains predominately protonated under these conditions. Similar observations have been reported for structurally related complexes [44]. After drying the product under high vacuum, the complexes were recrystallised from a solution of dry ethanol and diethyl ether, yielding pure **1a**, **1b**, and **1c** in moderate to good yields of 51–74%.

In addition to pH variation of the reaction mixture to push the equilibrium from *N,O*- to *N,N*-coordination or *vice versa*, the temperature has been shown to affect the isomerization in related compounds [44]. At temperatures below −20 °C, *N,O*-coordination was favored but above 50 °C it shifted towards *N,N*-coordination. In the case of complex **1a**, heating the reaction mixture at 40–60 °C for 12 h at pH 3 still exclusively led to *N,O*-coordination suggesting that pH effects may override temperature effects. The different halido ligands in **1a**–**1c** not only impact the ligand exchange properties of the complexes but also the coordination mode of **1** to the Ru center. After 15 days in methanol, **1a** and **1b** showed no sign of conversion to *N,N*-coordination while such was detected for **1c** after 48 h and a ratio of 1 : 1 was reached within 6 d and remained constant for 4 weeks. Studies at room temperature and under heating suggest that as the halido ligand size increases, *N,O* coordination becomes less favorable.

Comparison of the ^{1}H NMR spectra of **1a**–**1c** to that of **1** revealed that coordination of ruthenium to **1** induced significant downfield shifts of the pyridine proton H1 from about 8.6 to 9.5 ppm (Fig. S3). The *N*-CH_2 protons in **1** are chemically equivalent but upon coordination to Ru became diastereotopic. In addition, the spectra featured all the peaks expected for the *p*-cymene ligand.

Single crystals of **1a** were obtained by slow diffusion of diethyl ether into a solution of **1a** in methanol. The complex crystalized in a monoclinic crystal system with a $P2_1/c$ space group. The molecular structure confirmed that the ligand was coordinated to Ru bidentately *via* its pyridyl nitrogen N1 and amide oxygen O1 atoms (Fig. 2). The coordination of **1** to ruthenium results in an asymmetric complex, and the molecular structure featured an

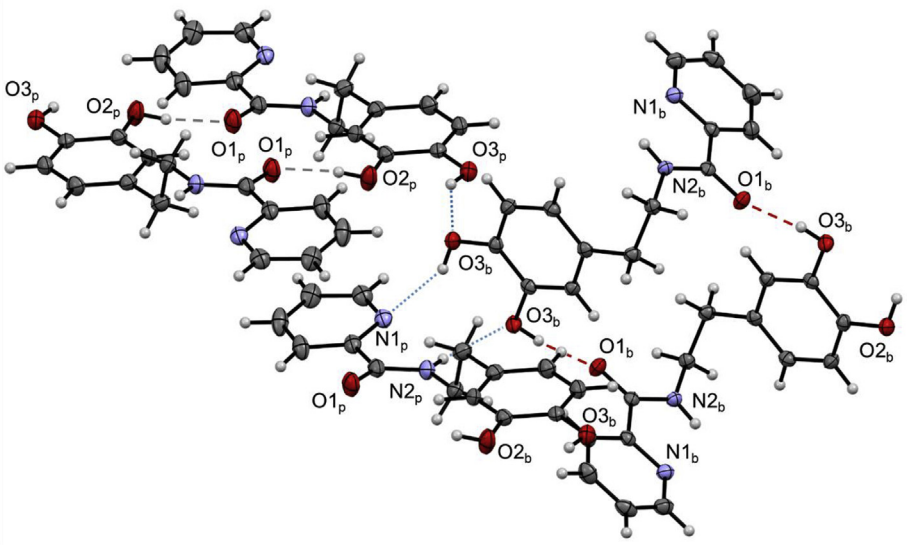

Fig. 1. Molecular structures of four molecules of **1** drawn at 50% probability level. Hydrogen bonds between bent molecules are indicated as red long dashed lines, between molecules with parallel phenyl and pyridine rings as grey long dashed lines and between the two types of molecules as blue short dashed lines. (For interpretation of the references to color in this figure legend, the reader is referred to the Web version of this article.)

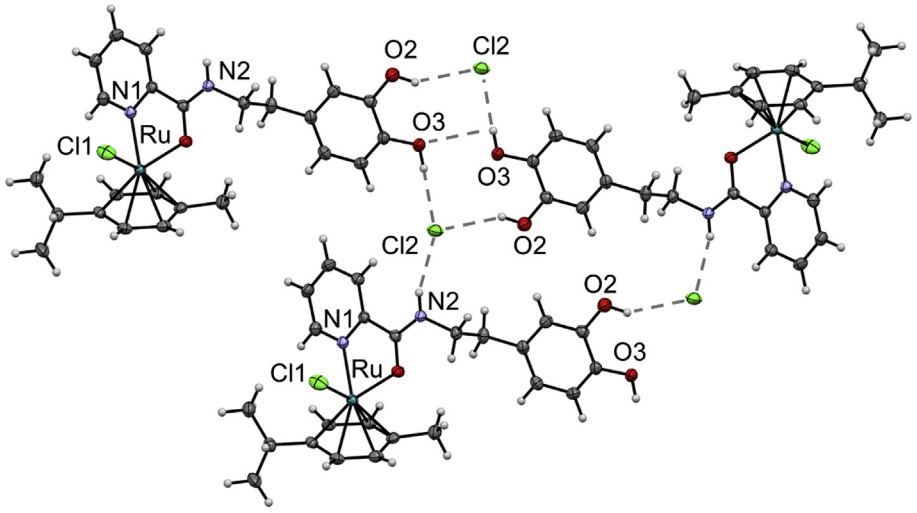

Fig. 2. Molecular structure of **1a** drawn at 50% probability levels. Hydrogen bonds are depicted as grey dashed lines.

enantiomeric mixture of the compound as observed for related structures [33]. The molecular structure featured a chloride counterion, supporting that the amide proton remains protonated under the conditions used which results in the presence of a complex cation. Similar to ligand **1**, extensive hydrogen bonding was found involving the catechol hydroxyl groups, the amide proton and chloride counterions of both enantiomers in the structure. However, given the coordination of the Ru center to the picolinamide moiety, the number of hydrogen bonds was reduced as compared to the structure of **1**. In addition, π interactions (3.469 Å) formed between the two enantiomers through their pyridyl and phenyl groups (Fig. S4).

The molecular structure of **1b** was very similar to that of **1a**. A slight disorder of the bromide counterion was observed influencing the positioning of the catechol O2–H hydrogen atom and therewith the O2–H···Br^- hydrogen bond (Figs. S5 and S6). Comparison of selected bond lengths (Table 1) demonstrates that coordination of the metal center had a significant impact on the bond lengths found for the amide group, with the C6=O1 bond extended upon coordination and the C6–N2 distance shortened. This is consistent with coordination to the amide oxygen O1 inducing more single bond character in the C6=O1 bond, while the C6–N2 bond obtains more double bond character (see Table 1).

Table 1
Selected bond lengths (Å) in the structures of **1**, **1a** and **1b**.

Bond	1	1a $^{X=Cl}$	1b $^{X=Br}$
C6=O1	1.2441(16)	1.262(3)	1.255(4)
C6–N2	1.3300(17)	1.314(3)	1.317(4)
Ru–X1	–	2.3828(7)	2.5167(5)
Ru–O1	–	2.0881(17)	2.095(2)
Ru–N1	–	2.119(2)	2.118(3)

Table 2
X-ray diffraction analysis data for **1**, **1a** and **1b**.

Compound	**1**	**1a**	**1b**
CCDC	1885727	1885728	1885729
Chemical Formula	$C_{14}H_{14}N_2O_3$	$C_{24}H_{28}Cl_2N_2O_3Ru$	$C_{24}H_{27}Br_2N_2O_3Ru$
M (g mol^{-1})	258.27	564.45	652.37
Temperature (K)	100(2)	100(2)	100(2)
Crystal size (mm)	0.34 × 0.32 × 0.10	0.34 × 0.22 × 0.14	0.36 × 0.10 × 0.10
Crystal system	triclinic	monoclinic	monoclinic
Space group	*P*-1	$P2_1/c$	$P2_1/c$
a (Å)	7.6311(2)	10.2791(3)	10.5324(2)
b (Å)	9.2666(2)	11.0850(4)	11.0839(2)
c (Å)	17.6831(4)	21.2650(6)	21.4446(4)
α (°)	91.665(1)	90	90
β (°)	91.844(1)	103.102(1)	103.402(1)
γ (°)	96.104(1)	90	90
V (A^3)	1242.05(5)	2359.94(13)	2435.27(8)
Z	4	4	4
D_c (mg m^{-3})	1.381	1.589	1.782
μ (mm^{-1})	0.099	0.920	3.954
F (000)	544	1152	1296
Θ range (deg)	2.21 to 27.91	1.97 to 27.88	1.99 to 25.50
h range	$-9 \le h \le 9$	$-13 \le h \le 11$	$-12 \le h \le 12$
k range	$-12 \le k \le 12$	$-14 \le k \le 13$	$-13 \le k \le 11$
l range	$-23 \le l \le 23$	$-27 \le l \le 27$	$-25 \le l \le 25$
Reflections collected	26245	26729	23960
Data/restraints/parameters	5858/0/347	5547/0/298	4519/2/306
Independent reflections (R_{int})	5858 (0.0546)	5547 (0.0515)	4519 (0.0543)
R_1, wR_2 (obs., $I \ge 2\sigma$ (I))	0.0426, 0.1002	0.0331, 0.0763	0.0328, 0.0684
R_1, wR_2 (all data)	0.0628, 0.1123	0.0428, 0.0815	0.0455, 0.0733
S on F^2	1.045	1.046	1.037

2.1. N,O- vs. N,N-coordination — DFT calculations

As we observed a mixture of products in the ^{1}H NMR spectra, we used DFT calculations to investigate the preference for *N,O*- over *N,N*-coordination and compared different protonated and deprotonated, and therewith charged or neutral, derivatives of **1a** (Fig. S7). When comparing the protonated and the deprotonated forms of the *N,O*- and *N,N*-coordinated derivatives, *i.e.*, $\mathbf{1a}^{N,O}{}_{prot}$ *vs.* $\mathbf{1a}^{N,O}{}_{deprot}$ and $\mathbf{1a}^{N,N}{}_{prot}$ *vs.* $\mathbf{1a}^{N,N}{}_{deprot}$, the deprotonated form was energetically favored by 86.7 and 66.4 kcal mol^{-1}. When looking for preference of *N,O*- over *N,N*-coordination, as observed in the molecular structures of **1a** and **1b**, the former was 12.7 kcal mol^{-1} lower in energy. This supports that **1** acts preferably as a bidentate *N,O*-donor chelator, but also shows that the energy difference is not huge and therefore it is not surprising to find in solution the formation of both *N,O* and *N,N*-chelated ligand.

Calculation of the frontier orbitals of $\mathbf{1a}^{N,O}{}_{prot}$ showed that LUMO and LUMO+1 were located largely at the pyridine ring and metal center, while HOMO-1 and HOMO were found at the catechol moiety. Deprotonation of $\mathbf{1a}^{N,O}{}_{prot}$ to $\mathbf{1a}^{N,O}{}_{deprot}$ shifted the HOMO orbitals more towards the metal center, in particular involving the amide group.

In the case of *N,N*-coordination, the HOMO-1 of $\mathbf{1a}^{N,N}{}_{prot}$ was found at the metal center while the HOMO, LUMO and LUMO+1 were at the catechol moiety as in $\mathbf{1a}^{N,O}{}_{prot}$. Deprotonation affected the HOMOs significantly and the HOMO-1 was now mainly centered at the catechol, while the HOMO was located at the Ru and the amidate group. The LUMOs were again similar to the other cases.

3. Nanoparticle functionalization

To coordinate complexes **1a**–**1c** to the Fe ions in the Fe_3O_4 NPs (NPs; 9.4 nm), the catechol group was deprotonated with an excess of sodium methoxide in methanol allowing for binding to the NPs through displacement of the betaine capping. After 24 h of shaking the reaction mixture containing the complexes, NaOMe and NPs, the latter were washed at least 5 times with methanol to remove any unbound complex. Various ratios of Ru complex to NPs were explored ranging from 0.25- to 5-fold predicted surface coverage considering the NPs as spherical structures (Supporting Information). Inductively-coupled plasma mass spectrometry (ICP-MS) was used to determine the amount of Ru relative to the Fe content of the NPs. These studies demonstrated that loading of **1a**–**1c** was independent of the halido leaving ligand (Fig. 3), supporting rapid ligand exchange kinetics under the conditions used. It was expected that a plateau should be reached when the NP surface becomes fully saturated with the Ru complexes. However, this was not observed and the NP loading continued to increase with increasing Ru : Fe ratios, indicating that there may be other interactions and possible formation of multilayers of Ru complexes. This may occur through electrostatic interactions or the catecholate may coordinate to already surface- bound complexes and increase

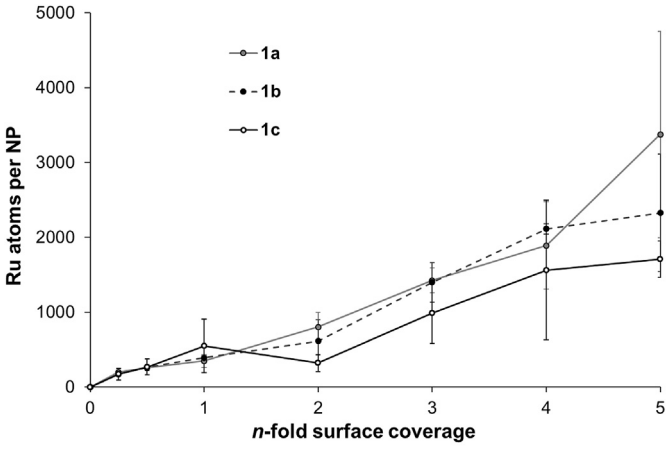

Fig. 3. ICP-MS data analysis of Fe_3O_4 nanoparticles loaded with **1a**–**1c** at concentrations to reach surface coverage levels of 0.25–5x.

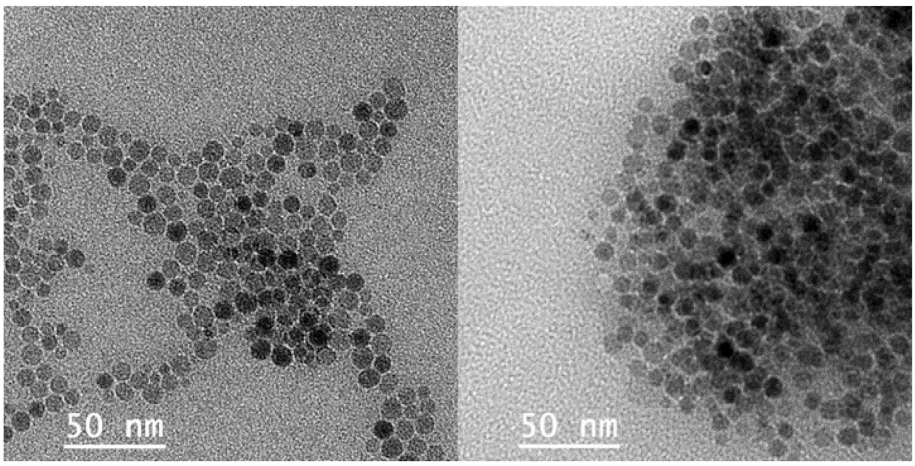

Fig. 4. TEM analysis of NPs (left) and NPs reacted with **1a** (right).

the loading of the NPs with Fe.

Fourier transform infra-red (FTIR) spectroscopy was used to confirm deprotonation of the catechol group of **1b** and coordination to the NP Fe ions (Fig. S8). The FTIR spectrum of **1b** showed two vibrational frequencies at 1600 and 1624 cm^{-1}, corresponding to amide N–H and C=O bonds, respectively. In addition, broad peaks in the range 3000–3300 cm^{-1} are indicative of the presence of OH groups. The FTIR spectra of Fe_3O_4 NPs showed a broad band at 3500 cm^{-1}, suggesting the presence of surface hydroxyl groups [49], while a sharp peak at 575 cm^{-1} relates to the iron oxide core [50]. Upon loading **1b** onto the NPs, the peaks at 3100–3300 cm^{-1} were absent, while the carbonyl of **1b** was detected at about 1600 cm^{-1}. This supports that binding between **1b** and the Fe_3O_4 NPs occurred *via* catecholate formation.

Size and morphology of the NPs were studied using transmission electron microscopy (TEM). Coating Fe_3O_4 nanoparticles prevents aggregation, while uncoated NPs tend to aggregate due to hydrophobic interactions. Upon treatment with **1a**, the TEM images indicated that the nanoparticle size was not affected (Fig. 4). The morphology of the loaded nanoparticles did not change and individual spherical nanoparticles were observed.

4. Conclusions

With the aim to load an organometallic compound on magnetite NPs, the picolinamide derivative **1** with a catechol group was coordinated to Ru(cym)X (X = Cl, Br, I) in an *N*,*O*-coordination mode. Preference for the latter over *N*,*N*-coordination was established by performing DFT calculations. Experimentally, coordination through the *N*,*O*-donor system was achieved by acidifying the reaction mixture with acetic acid, however, other reaction conditions and also the nature of the halido group have an impact on the coordination mode. Several derivatives of the series were characterized by single crystal X-ray diffraction analysis.

Complexes **1a**–**1c** were loaded on Fe_3O_4 NPs by addition of base to deprotonate the catechol hydroxyl groups. The functionalized NPs were characterized by ICP-MS, FTIR spectroscopy, and TEM. ICP-MS revealed the ratio of Ru : Fe to increase with increasing Ru concentrations to cover the surface of the NPs independent of the halido ligand with no saturation of ruthenium observed for the concentration range used. The morphology and size of the nanoparticles were analyzed using TEM which showed that there was no visible difference in size between loaded and non-functionalized NPs, and the NPs did not aggregate. Bonding through catecholato ligands to the NPs was demonstrated by FTIR spectroscopy as indicated by the disappearance of O-H vibrational frequencies of the hydroxyl functional groups. Therefore, this approach was found to be viable to load organometallics effectively to magnetite NPs and could be used in future for the delivery of anticancer agents.

5. Experimental

5.1. Material and methods

All air sensitive reactions were carried out under nitrogen (N_2) flow in standard Schlenk flasks. Dopamine hydrochloride, 2-pyridinocarboxaldehyde and picolinic acid were purchased from Sigma-Aldrich and iron oxide nanoparticles (9.4 ± 1.2 nm in aqueous solution) capped with betaine·HCl were kindly provided by Boutiq (New Zealand). Reactions involving light-sensitive material were performed in the darkness using aluminum foil to prevent oxidation. All solid reagents were dried in Schlenk flasks under high vacuum for a minimum of 12 h prior to use. Dichloromethane, ethanol, and diethyl ether were collected from a solvent purification system (LC Technology Solutions Inc., Sp-1 solvent purifier) and transferred to a dry Schlenk flask following purging with N_2 gas. Dimethylformamide and methanol were first dried over activated molecular sieves (3 Å) under N_2 for 48 h prior to use. Thin layer chromatography (TLC) was performed on aluminum sheets pre-coated with Merck silica gel 60 F254. Flash column chromatography was performed on a CombiFlashRF200 using BUCHI plastic and glass columns. Solvents used for flash column chromatography were of HPLC grade and used without further purification. The dimeric Ru precursors bis-[dichlorido(η^6-*p*-cymene)ruthenium(II)] [51], bis[dibromido(η^6-*p*-cymene)ruthenium(II)], bis[diiodido(η^6-*p*-cymene)ruthenium(II)] [52] were synthesized by adapting reported procedures.

Melting points were determined on a Bibby Stuart Scientific Melting Point Apparatus SMP3 using capillary tubes. ^1H and $^{13}C\{^1H\}$ DEPT-Q NMR spectra were recorded at 25 °C using a Bruker DRX 400 MHz NMR spectrometer at 400.13 and 100.61 MHz, respectively. High resolution mass spectroscopy data was recorded on a Bruker micrOTOF-QII mass spectrometer in positive ESI mode.

The X-ray diffraction data of crystals of **1**, **1a** and **1b** were collected on a Bruker Smart APEX II diffractometer with graphite-monochromatized Mo Kα radiation (λ = 0.71073 Å) at 100 K (Table 2). Data reduction was carried out using the SAINT program [53]. Semi-empirical absorption corrections were applied based on equivalent reflections using SADABS [54]. The structure solution

and refinements were performed with the SHELXS-97 and SHELXL-2016 program packages [55].

5.2. Syntheses

5.2.1. Synthesis of N-(3,4-dihydroxyphenethyl)picolinamide (**1**)

A solution of 3,4-dihydroxyphenethylamine hydrochloride (460 mg, 3.00 mmol) in 10 mL dry methanol (neutralized with sodium methoxide) was added to a solution of 2-pyridinecarboxylic acid (388 mg, 3.15 mmol) and HATU (1269 mg, 3.34 mmol) in DMF (20 mL). The pale-yellow solution was stirred for 20 min at room temperature. Then DIPEA (608 mg, 0.82 mL, 4.72 mmol) was added and the resulting yellow solution was stirred for 48 h at room temperature under light protection. Afterwards DMF was evaporated, the waxy gel like residue was dissolved in ethyl acetate and washed with water (3 × 25 mL) followed by an aqueous saturated $NaHCO_3$ solution (3 × 25 mL). The aqueous layers were combined and washed with ethyl acetate (3 × 15 mL). The ethyl acetate fractions were combined and dried with anhydrous Na_2SO_4, filtered and the solvent was evaporated to give a brown oil. The oil was purified by flash column chromatography over silica (ethyl acetate: hexane = 2 : 1) which yielded a colorless liquid. The liquid was dried under high vacuum to give a white solid. Yield 155 mg (37%). Melting point: 99–101 °C. MS (ESI^+): *m/z* 259.1073 $[M + H]^+$ (m/z_{calc} 259.1083); *m/z* 281.0891 $[M + Na]^+$ (m/z_{calc} 281.0902). ^1H NMR (400.13 MHz, CD_3OD): $\delta = 8.58$ (dt, $^3J = 5$ Hz, $^4J = 1$ Hz, 1H, H-1), 8.06 (dt, $^3J = 8$ Hz, $^4J = 1$ Hz, 1H, H-2), 7.92 (td, $^3J = 8$ Hz, $^4J = 1$ Hz, 1H, H-3), 7.58 (ddd, $^3J = 5$ Hz, $^4J = 1$ Hz, 1H, H-2), 6.67–6.69 (m, 2H, H-13, H-10), 6.57 (dd, $^3J = 8$, $^4J = 2$, 1H, H-14), 3.58 (t, $^3J = 8$, 2H, H-7), 2.75 (t, $^3J = 6$, 2H, H-8) ppm; $^{13}C\{^1H\}$ NMR (100.61 MHz, CD_3OD): δ = 166.6 (C-6), 151.1 (C-5), 149.8 (C-1), 146.3 (C-11), 144.9 (C-12), 138.7 (C-3), 131.9 (C-9), 127.7 (C-2), 123.0 (C-4), 121.1 (C-14), 117.0 (C-10), 116.5 (C-13), 34.3 (C-7), 36.1 (C-8) ppm.

5.2.2. [Chlorido{N-(3,4-dihydroxyphenethyl)picolinamide}(η^6-*p*-cymene)ruthenium(II)]chloride **1a**

A solution of $[RuCl_2(\eta^6\text{-}p\text{-cymene})]_2$ (49 mg, 0.08 mmol) in dry methanol (8 mL) was added to **1** (41 mg, 0.16 mmol), followed by dropwise addition of acetic acid till the solution reached pH 3 and refluxed overnight in darkness. The solvent was then removed, the residue dissolved in minimal amounts of dry ethanol (2 mL) and precipitated out with dry ethyl ether (12 mL). The precipitate was filtered and collected yielding a red solid. Yield: 57 mg (63%), Melting point: 185–187 °C (decomp.). MS (ESI^+): *m/z* 493.1063 $[M - H - 2Cl]^+$ (m/z_{calc} 493.1066). ^1H NMR (400.13 MHz, CD_3OD): $\delta = 9.46$ (dt, $^3J = 5$ Hz, $^4J = 1$ Hz, 1H, H-1), 8.29 (dt, $^3J = 8$ Hz, $^4J = 1$ Hz, 1H, H-3), 8.24 (d, $^3J = 7$ Hz, 1H, H-4), 7.93 (dt, $^3J = 7$ Hz, $^4J = 2$ Hz, 1H, H-2), 6.74–6.68 (m, 2H, H-10, H-13), 6.58 (d, $^3J = 8$, 1H, H-14), 5.96 (d, $^3J = 6$, 1H, H-16/H-20), 5.94 (d, $^3J = 6$, 1H, H-16/H-20), 5.80 (d, $^3J = 6$ Hz, 1H, H-17/H-19), 5.70 (d, $^3J = 6$ Hz, 1H, H-17/H-19), 3.86–3.90 (m, 1H, H-7), 3.68–3.71 (m, 1H, H-7), 2.92–2.78 (m, 3H, H-8, H-22), 2.29 (s, 3H, H-21), 1.27 (d, $^3J = 7$ Hz, 6H, H-23, H-24) ppm; $^{13}C\{^1H\}$ NMR (100.61 MHz, CD_3OD): δ = 170.5 (C-6), 154.9 (C-1), 147.8 (C-5), 145.0 (C-11), 143.9 (C-12), 141.5 (C-3 or C-4), 130.9 (C-2), 130. 8 (C-3 or C-4), 123.7 (C-9), 120.3 (C-14), 116.4 (C-10), 116.1 (C-13), 104.2 (C-15), 99.9 (C-18), 83.3, 83.5, 80.4, 79.3 (C-16, C-17, C-19, C-20), 43.1 (C-7), 35.5 (C-22), 32.7 (C-8), 22.3, 21.2 (C-23, C-24), 18.9 (C-21) ppm.

5.2.3. [Bromido{N-(3,4-dihydroxyphenethyl)picolinamide}(η^6-*p*-cymene)ruthenium(II)]bromide **1b**

A solution of $[RuBr_2(\eta^6\text{-}p\text{-cymene})]_2$ (50 mg, 0.063 mmol) in dry methanol (8 mL) was added to **1** (32 mg, 0.13 mmol) followed by dropwise addition of acetic acid till the solution reached pH 3 and refluxed overnight in darkness. The solvent was then removed, the residue dissolved in minimal amounts of dry ethanol (2 mL) and precipitated out with dry ethyl ether (12 mL). The precipitate was filtered and collected yielding a dark green-yellow solid. Yield: 42 mg (51%). Melting point: 195–200 °C (decomp.). MS (ESI^+): *m/z* 573.0337 $[M - Br]^+$ (m/z_{calc} 573.0323), *m/z* 493.1066 $[M - H - 2Br]^+$ (m/z_{calc} 493.1066). ^1H NMR (400.13 MHz, CD_3OD): $\delta = 9.40$ (dt, $^3J = 5$ Hz, $^4J = 1$ Hz, 1H, H-1), 8.21–8.28 (m, 2H, H-3, H-4), 7.91 (td, $^3J = 7$ Hz, $^4J = 2$ Hz, H1, H-2), 6.69–6.72 (m, 2H, H-10, H-13), 6.57 (dd, $^3J = 8$ Hz, $^4J = 2$ Hz, 1H, H-14), 5.88–5.92 (m, 2H, H-16, H-20), 5.79 (d, $^3J = 6$ Hz, 1H, H-17/19), 5.68 (d, $^3J = 6$ Hz, 1H H-17/19), 3.81–3.88 (m, 1H, H-7), 3.66–3.72 (m, 1H, H-7), 2.75–2.92 (m, 3H, H-8, H-22), 2.32 (s, 3H, H-21), 1.27 (d, $^3J = 6$ Hz, 6H, H-23/H-24) ppm; $^{13}C\{^1H\}$ NMR (100.61 MHz, CD_3OD): δ = 170.4 (C-6), 155.3 (C-1), 147.9 (C-5), 145.0 (C-11), 143.7 (C-12), 140.0 (C-3 or C-4), 129.8 (C-3 or C-4, C-2), 124.0 (C-9), 120.0 (C-14), 115.6 (C-10), 115.0 (C-13), 104.0 (C-15), 98.2 (C-18), 82.6, 82.5, 82.0, 81.1 (C-16, C-17, C-19, C-20), 42.8 (C-7), 33.8 (C-22), 31.2 (C-8), 21.0–20.9 (C-23, C-24), 17.6 (C-21) ppm.

5.2.4. [Iodido{N-(3,4-dihydroxyphenethyl)picolinamide}(η^6-*p*-cymene)ruthenium(II)]iodide **1c**

A solution of $[RuI_2(\eta^6\text{-}p\text{-cymene})]_2$ (38 mg 0.04 mmol) in dry methanol (16 mL) was added to **1** (20 mg, 0.08 mmol) followed by dropwise addition of acetic acid till the solution reached pH 3 and refluxed overnight in darkness. The solvent was then removed, the residue dissolved in minimal amounts of dry ethanol (2 mL) and precipitated out with dry ethyl ether (14 mL). The precipitate was filtered and collected yielding an orange solid. Yield: 43 mg (74%). Melting point: 200–204 °C (decomp.). MS (ESI^+): *m/z* 621.0208 $[M - I]^+$ (m/z_{calc} 621.0189). ^1H NMR (400.13 MHz, CD_3OD): $\delta = 9.2$ (dt, $^3J = 5$ Hz, $^4J = 1$ Hz, 1H, H-1), 8.17–8.23 (m, 2H, H-3, H-4), 7.85 (td, $^3J = 7$ Hz, $^4J = 2$ Hz, 1H, H-2), 6.66–6.69 (m, 2H, H-10, H-13), 6.54 (d, $^3J = 8$ Hz, 1H, H-14), 5.84–5.89 (m, 2H, H-16, H-20), 5.79 (d, $^3J = 6$ Hz, 1H, H-17/19) 5.68 (d, $^3J = 6$ Hz, 1H, H-17/19), 3.75–3.83 (m, 1H, H-7), 3.66–3.72 (m, 1H, H-7), 2.84–2.93 (m, 2H, H-8), 2.73–2.80 (m, 1H, H-22), 2.34 (s, 3H, H-21), 1.26 (d, $^3J = 5$ Hz, 6H, H-23, H-24) ppm; $^{13}C\{^1H\}$ NMR (100.61 MHz, CD_3OD): δ = 171.5 (C-6), 157.6 (C-1), 149.4 (C-5), 146.5 (C-11), 145.2 (C-12), 141.4 (C-3 or C-4), 131.3 (C-2), 131.1(C-3 or C-4), 125.5 (C-9), 121.5 (C-14), 117.1 (C-10), 116.4 (C-13), 106.4 (C-15), 98.8 (C-18), 84.4, 84.3, 83.7, 83.0 (C-16, C-17, C-19, C-20), 44.2 (C-7), 35.4 (C-22), 32.9 (C-8), 22.6, 22.5 (C-23, C-24), 19.7 (C-21) ppm.

6. DFT calculations

Gaussian 09 [56] was used to calculate the optimized ground state structures and frequencies for the different molecules by density functional theory (DFT) with the B3LYP hybrid exchange functional and a split basis set for C, H, N, O, Cl (6-31G(d,p)) and the transition metal ruthenium (SDDAll) in vacuum. The frontier orbitals were visulalized with the Avogadro software (version 1.2.0) [57].

7. Nanoparticle functionalization

A stock solution of Ru complex (**1a**–**1c**) and sodium methoxide was prepared to give a concentration of 10 mg mL^{-1} in methanol (approximately 1 mL). Suspensions of NPs (50 mg mL^{-1}, 20 μL, 9.4 nm) and methanol (900 μL) were added to a series of tubes to which increasing concentrations of Ru complexes and sodium methoxide were added (2 mol equiv.). The samples were shaken on an orbital shaker at 300 rpm for 24 h at room temperature. The NPs were separated from unreacted Ru complexes by centrifugation (140000 rpm, 5 min) and decanting the solutions. The NPs were then resuspended in methanol (900 μL) and centrifuged (140000 rpm, 5 min), and these washing steps were repeated five

times. Afterwards the samples were dried under high vacuum overnight and stored in the fridge until analysis with ICP-MS and TEM.

8. Inductively coupled plasma mass spectrometry

The NP conjugates (1 mg mL^{-1}) were prepared for ICP-MS analysis by open vessel digestion with HNO_3 (2.4 mL, 69%) and HCl (1.6 mL, 37%) so that the total acid ratio 3 : 2 in 15 mL tubes. Then the samples were serially diluted with 8 mL water (18.2 MΩ) and 2.5 mL was taken and further diluted with 5 mL water (18.2 MΩ) to achieve a final HNO_3 concentration of 4.6% HNO_3 and 1.6% HCl.

An Agilent 7700 inductively coupled plasma-quadrupole mass spectrometer (ICP-MS) was used to quantify the ^{101}Ru and ^{56}Fe content of the NP conjugates. Unmodified nanoparticle samples were used as controls. ^{115}In (0.5 ppb) was added to the digestion mixture to trace the amount of metal lost during digestion, while ^{159}Tb (20 ppb) was monitored as an internal standard for instrument drift/stability.

Ru and Fe solutions (1000 ppm stock, Peak Performance CPI international) in 4.6% HNO_3 and 1.6% HCl were used to calibrate the instrument with standards of 0.05, 0.25, 0.5, 2.5 and 5.0 ppb for Fe and 0.01, 0.05, 0.1, 0.5 and 1.0 ppb for Ru.

9. Transmission electron microscopy

Transmission electron microscopy (TEM) was conducted on 120 kV FEI Tecnai 12 or 200 kV FEI Tecnai FEG20 (TF20) TEMs using Gatan Ultrascan 1000 (4 MP) cameras and images were processed with Gatan digital micrograph software. The nanoparticle conjugates were prepared for TEM by suspending and sonicating them in methanol (1 mg mL^{-1}) and then 10 μL was taken and pipetted onto a copper TEM grid and air dried.

Acknowledgements

We thank the University of Auckland for financial support and the Imaging Centre at the Faculty of Science, of the University of Auckland for access to the TEM instruments. The authors are grateful to Tanya Groutso for collecting the X-ray crystal data, Tony Chen for ESI-MS analyses and Stuart Morrow for help with the ICP-MS measurements.

Appendix A. Supplementary data

Supplementary data to this article can be found online at https://doi.org/10.1016/j.jorganchem.2019.03.020.

References

[1] B.S. Murray, M.V. Babak, C.G. Hartinger, P.J. Dyson, Coord. Chem. Rev. 306 (2016) 86–114.
[2] C.S. Allardyce, P.J. Dyson, Dalton Trans. 45 (2016) 3201–3209.
[3] M. Hanif, C.G. Hartinger, Future Med. Chem. 10 (2018) 615–617.
[4] A.A. Nazarov, C.G. Hartinger, P.J. Dyson, J. Organomet. Chem. 751 (2014) 251–260.
[5] J.M. Gichumbi, H.B. Friedrich, J. Organomet. Chem. 866 (2018) 123–143.
[6] A.D. Liang, J. Serrano-Plana, R.L. Peterson, T.R. Ward, Acc. Chem. Res. 52 (3) (2019) 585–595.
[7] R. Matheu, M.Z. Ertem, C. Gimbert-Surinach, X. Sala, A. Llobet, Chem. Rev. 119 (6) (2019) 3453–3471.
[8] P. Thangavel, B. Viswanath, S. Kim, Int. J. Nanomed. 12 (2017) 2749–2758.
[9] J. Suriboot, H.S. Bazzi, D.E. Bergbreiter, Polymers 8 (2016) 140.
[10] F.-A. Khan, G. Süss-Fink, Eur. J. Inorg. Chem. 2012 (2012) 727–732.
[11] L. Wu, Y.-M. He, Q.-H. Fan, Adv. Synth. Catal. 353 (2011) 2915–2919.
[12] L. Rosado Piquer, E. Jiménez Romero, Y. Lan, W. Wernsdorfer, G. Aromí, E.C. Sañudo, Inorg. Chem. Front. 4 (2017) 595–603.
[13] R.J. Holmberg, A.-J. Hutchings, F. Habib, I. Korobkov, J.C. Scaiano, M. Murugesu, Inorg. Chem. 52 (2013) 14411–14418.
[14] S. Laurent, D. Forge, M. Port, A. Roch, C. Robic, L. Vander Elst, R.N. Muller, Chem. Rev. 108 (2008) 2064–2110.
[15] A. Ito, M. Shinkai, H. Honda, T. Kobayashi, J. Biosci. Bioeng. 100 (2005) 1–11.
[16] C. Corot, P. Robert, J.-M. Idée, M. Port, Adv. Drug Deliv. Rev. 58 (2006) 1471–1504.
[17] D.J. Thorek, A. Chen, J. Czupryna, A. Tsourkas, Ann. Biomed. Eng. 34 (2006) 23–38.
[18] J. Xie, J. Huang, X. Li, S. Sun, X. Chen, Curr. Med. Chem. 16 (2009) 1278–1294.
[19] T.M. Zagar, J.R. Oleson, Z. Vujaskovic, M.W. Dewhirst, O.I. Craciunescu, K.L. Blackwell, L.R. Prosnitz, E.L. Jones, Int. J. Hyperth. 26 (2010) 618–624.
[20] M. Franckena, Int. J. Hyperth. 28 (2012) 543–548.
[21] J. Wang, X. Wang, Y. Song, J. Wang, C. Zhang, C. Chang, J. Yan, L. Qiu, M. Wu, Z. Guo, Chem. Sci. 4 (2013) 2605–2612.
[22] Z. Zhu, Z. Wang, Y. Hao, C. Zhu, Y. Jiao, H. Chen, Y.-M. Wang, J. Yan, Z. Guo, X. Wang, Chem. Sci. 7 (2016) 2864–2869.
[23] C.S. Allardyce, P.J. Dyson, D.J. Ellis, S.L. Heath, Chem. Commun. (2001) 1396–1397.
[24] L. Ren, X.-L. Huang, B. Zhang, L.-P. Sun, Q.-Q. Zhang, M.-C. Tan, G.-M. Chow, J. Biomed. Mater. Res. A 85A (2008) 787–796.
[25] X. Wang, Z. Guo, Chem. Soc. Rev. 42 (2013) 202–224.
[26] S.D. Brown, P. Nativo, J.-A. Smith, D. Stirling, P.R. Edwards, B. Venugopal, D.J. Flint, J.A. Plumb, D. Graham, N.J. Wheate, J. Am. Chem. Soc. 132 (2010) 4678–4684.
[27] S. Bhattacharyya, M. Gonzalez, J.D. Robertson, R. Bhattacharya, P. Mukherjee, Chem. Commun. 47 (2011) 8530–8532.
[28] N.P.E. Barry, P.J. Sadler, Chem. Commun. 49 (2013) 5106–5131.
[29] S. Seršen, J. Kljun, K. Kryeziu, R. Panchuk, B. Alte, W. Körner, P. Heffeter, W. Berger, I. Turel, J. Med. Chem. 58 (2015) 3984–3996.
[30] C.A. Vock, C. Scolaro, A.D. Phillips, R. Scopelliti, G. Sava, P.J. Dyson, J. Med. Chem. 49 (2006) 5552–5561.
[31] M. Hanif, M.A.H. Nawaz, M.V. Babak, J. Iqbal, A. Roller, B.K. Keppler, C.G. Hartinger, Molecules 19 (2014) 8080–8092.
[32] R. Pettinari, F. Marchetti, F. Condello, C. Pettinari, G. Lupidi, R. Scopelliti, S. Mukhopadhyay, T. Riedel, P.J. Dyson, Organometallics 33 (2014) 3709–3715.
[33] M. Kubanik, H. Holtkamp, T. Sohnel, S.M.F. Jamieson, C.G. Hartinger, Organometallics 34 (2015) 5658–5668.
[34] J. Kljun, A.K. Bytzek, W. Kandioller, C. Bartel, M.A. Jakupec, C.G. Hartinger, B.K. Keppler, I. Turel, Organometallics 30 (2011) 2506–2512.
[35] W.H. Ang, L.J. Parker, A. De Luca, L. Juillerat-Jeanneret, C.J. Morton, M. Lo Bello, M.W. Parker, P.J. Dyson, Angew. Chem., Int. Ed. Engl. 48 (2009) 3854–3857.
[36] G. Agonigi, T. Riedel, S. Zacchini, E. Păunescu, G. Pampaloni, N. Bartalucci, P.J. Dyson, F. Marchetti, Inorg. Chem. 54 (2015) 6504–6512.
[37] E. Păunescu, S. McArthur, M. Soudani, R. Scopelliti, P.J. Dyson, Inorg. Chem. 55 (2016) 1788–1808.
[38] F. Aman, M. Hanif, M. Kubanik, A. Ashraf, T. Sohnel, S.M.F. Jamieson, W.A. Siddiqui, C.G. Hartinger, Chem. Eur J. 23 (2017) 4893–4902.
[39] S.H. van Rijt, A.F.A. Peacock, R.D.L. Johnstone, S. Parsons, P.J. Sadler, Inorg. Chem. 48 (2009) 1753–1762.
[40] S.H. van Rijt, A. Mukherjee, A.M. Pizarro, P.J. Sadler, J. Med. Chem. 53 (2010) 840–849.
[41] S.J. Lucas, R.M. Lord, R.L. Wilson, R.M. Phillips, V. Sridharan, P.C. McGowan, Dalton Trans. 41 (2012) 13800–13802.
[42] Z. Almodares, S.J. Lucas, B.D. Crossley, A.M. Basri, C.M. Pask, A.J. Hebden, R.M. Phillips, P.C. McGowan, Inorg. Chem. 53 (2014) 727–736.
[43] A. Ashraf, M. Hanif, M. Kubanik, T. Sohnel, S.M.F. Jamieson, A. Bhattacharyya, C.G. Hartinger, J. Organomet. Chem. 839 (2017) 31–37.
[44] S.H. van Rijt, A.J. Hebden, T. Amaresekera, R.J. Deeth, G.J. Clarkson, S. Parsons, P.C. McGowan, P.J. Sadler, J. Med. Chem. 52 (2009) 7753–7764.
[45] J.M. Poljarević, G. Tamás Gál, N.V. May, G. Spengler, O. Dömötör, A.R. Savić, S. Grgurić-Šipka, É.A. Enyedy, J. Inorg. Biochem. 181 (2018) 74–85.
[46] M.J. Sever, J.J. Wilker, Dalton Trans. (2006) 813–822.
[47] P.C. Kunz, H. Meyer, J. Barthel, S. Sollazzo, A.M. Schmidt, C. Janiak, Chem. Commun. 49 (2013) 4896–4898.
[48] W.P. Griffith, Transition Met. Chem. 18 (1993) 250–256.
[49] S. Sharifi, S. Daghighi, M.M. Motazacker, B. Badlou, B. Sanjabi, A. Akbarkhanzadeh, A.T. Rowshani, S. Laurent, M.P. Peppelenbosch, F. Rezaee, Sci. Rep. 3 (2013) 2173.
[50] S. Mondini, C. Drago, A.M. Ferretti, A. Puglisi, A. Ponti, Nanotechnology 24 (2013) 105702.
[51] M.A. Bennett, A.K. Smith, J. Chem. Soc., Dalton Trans. (1974) 233–241.
[52] M.G. Mendoza-Ferri, C.G. Hartinger, A.A. Nazarov, R.E. Eichinger, M.A. Jakupec, K. Severin, B.K. Keppler, Organometallics 28 (2009) 6260–6265.
[53] SAINT, Area Detector Integration Software, Siemens Analytical Instruments Inc., Madison, WI, USA, 1995.
[54] G.M. Sheldrick, SADABS, Program for Semi-empirical Absorption Correction, University of Göttingen, Göttingen, Germany, 1997.
[55] G.M. Sheldrick, Acta Crystallogr. A: Found. Crystallogr. A64 (2008) 112–122.
[56] Gaussian 09, Revision A.02, M.J. Frisch, G.W. Trucks, H.B. Schlegel, G.E. Scuseria, M.A. Robb, J.R. Cheeseman, G. Scalmani, V. Barone, G.A. Petersson, H. Nakatsuji, X. Li, M. Caricato, A. Marenich, J. Bloino, B.G. Janesko, R. Gomperts, B. Mennucci, H.P. Hratchian, J.V. Ortiz, A.F. Izmaylov, J.L. Sonnenberg, D. Williams-Young, F. Ding, F. Lipparini, F. Egidi, J. Goings, B. Peng, A. Petrone, T. Henderson, D. Ranasinghe,

V.G. Zakrzewski, J. Gao, N. Rega, G. Zheng, W. Liang, M. Hada, M. Ehara, K. Toyota, R. Fukuda, J. Hasegawa, M. Ishida, T. Nakajima, Y. Honda, O. Kitao, H. Nakai, T. Vreven, K. Throssell, J.A. Montgomery, Jr., J.E. Peralta, F. Ogliaro, M. Bearpark., J.J. Heyd, E. Brothers, K.N. Kudin, V.N. Staroverov, T. Keith, R. Kobayashi, J. Normand, K. Raghavachari, A. Rendell, J.C. Burant, S.S Iyengar, J. Tomasi, M. Cossi, J.M. Millam, M. Klene, C. Adamo, R. Cammi, J.W. Ochterski, R.L. Martin, K. Morokuma, O. Farkas, J.B. Foresman, D.J. Fox, Gaussian, Inc., 2016. Wallingford CT.

[57] M.D. Hanwell, D.E. Curtis, D.C. Lonie, T. Vandermeersch, E. Zurek, G.R. Hutchison, J. Cheminf. 4 (2012) 17.